Cardiovasc Intervent Radiol (2016) 39:239–250
DOI 10.1007/s00270-015-1200-6

CLINICAL INVESTIGATION INTERVENTIONAL ONCOLOGY

First Delayed Resection Findings After Irreversible Electroporation (IRE) of Human Localised Renal Cell Carcinoma (RCC) in the IRENE Pilot Phase 2a Trial

Johann Jakob Wendler[1] · Jens Ricke[3] · Maciej Pech[3] · Frank Fischbach[3] · Julian Jürgens[3] · Sandra Siedentopf[4] · Albert Roessner[4] · Markus Porsch[1] · Daniel Baumunk[1] · Martin Schostak[1] · Jens Köllermann[2] · Uwe-Bernd Liehr[1]

Received: 6 May 2015 / Accepted: 7 August 2015 / Published online: 4 September 2015

Abstract

Introduction It is postulated that focal IRE affords complete ablation of soft-tissue tumours while protecting the healthy peritumoral tissue. Therefore, IRE may be an interesting option for minimally invasive, kidney-tissue-sparing, non-thermal ablation of renal tumours.

Aim With this current pilot study ("IRENE trial"), we present the first detailed histopathological data of IRE of human RCC followed by delayed tumour resection. The aim of this interim analysis of the first three patients was to investigate the ablation efficiency of percutaneous image-guided focal IRE in RCC, to assess whether a complete ablation of T1a RCC and tissue preservation with the NanoKnife system is possible and to decide whether the ablation parameters need to be altered.

Methods Following resection 4 weeks after percutaneous IRE, the success of ablation and detailed histopathological description were used to check the ablation parameters.

Results The IRE led to a high degree of damage to the renal tumours (1 central, 2 peripheral; size range 15–17 mm). The postulated homogeneous, isomorphic damage was only partly confirmed. We found a zonal structuring of the ablation zone, negative margins and, enclosed within the ablation zone, very small tumour residues of unclear malignancy.

Jens Köllermann and Uwe-Bernd Liehr have contributed equally.

Johann Jakob Wendler, Jens Ricke, Maciej Pech, Frank Fischbach and Uwe-Bernd Liehr are with the German Academy for Microtherapy (DAfMT).
Daniel Baumunk, Martin Schostak, Jens Köllermann and Uwe-Bernd Liehr are with the Working Group for Focal and Microtherapy of the Academy for German Urologists.

✉ Johann Jakob Wendler
johann.wendler@med.ovgu.de

Jens Ricke
jens.Ricke@med.ovgu.de

Maciej Pech
macej.pech@med.ovgu.de

Frank Fischbach
frank.fischbach@med.ovgu.de

Julian Jürgens
julian.juergens@med.ovgu.de

Sandra Siedentopf
sandra.siedentopf@med.ovgu.de

Albert Roessner
albert.roessner@med.ovgu.de

Markus Porsch
markus.porsch@med.ovgu.de

Daniel Baumunk
daniel.baumunk@med.ovgu.de

Martin Schostak
martin.schostak@med.ovgu.de

Jens Köllermann
jens.koellermann@sana.de

Uwe-Bernd Liehr
uwe-bernd.liehr@med.ovgu.de

[1] Department of Urology, University Hospital, Otto von Guericke University of Magdeburg, Leipziger Str. 44, 39120 Magdeburg, Germany

[2] Institute of Pathology, Sana Klinikum Offenbach Am Main, Offenbach Am Main, Germany

[3] Department of Radiology, University of Magdeburg, Magdeburg, Germany

[4] Institute of Pathology, University of Magdeburg, Magdeburg, Germany

Conclusion According to these initial, preliminary study results of the first three renal cases, a new zonal distribution of IRE damage was described and the curative intended, renal saving focal ablation of localised RCC below <3 cm by percutaneous IRE by the NanoKnife system appears to be possible, but needs further, systematic evaluation for this treatment method and treatment protocol.

Keywords Irreversible electroporation (IRE) · Renal cell carcinoma (RCC) · Small renal mass (SRM) · Kidney · Focal therapy (FT) · Ablation

Introduction

In the treatment of RCC, focal therapy (FT) with the goal of minimising damage to the surroundings while still achieving total destruction of the tumour tissue is receiving increasing attention [1–4]. For focal IRE, it has been postulated that complete ablation of soft-tissue tumours with protection of the healthy peritumoral tissue is possible [2, 5–12]. Therefore, IRE represents an interesting potential option for nephron-sparing treatment of renal tumours. However, there is still a lack of clinical data for its application in RCC [13–16], and most studies have been based on radiological or post-biopsy assessment only. With this pilot study [17], we present the first detailed histopathological data of IRE treated RCC followed by delayed resection. The aims of the present interim analysis of the first three patients were to evaluate the ablation efficacy and accuracy of percutaneous focal IRE in RCC and to obtain a preliminary assessment of whether a histologically complete ablation of localised RCC with preservation of kidney tissue, using the NanoKnife™ system, is possible and to decide whether the ablation parameters need to be altered.

Methods

Study Approval

The detailed study protocol was published separately [17]. Approval for this GCP-compliant study [ClinicalTrials.gov: NCT01967407 (10/2013), ICTRP/WHO: DRKS00004266] was granted by German Federal Institute for Drugs and Medical Devices (BfArM) and Ethics Committee of University Magdeburg [73/2012].

Procedures

Metastatic disease was excluded by contrast-enhanced, thoracic CT and abdominopelvic CT or MRI. Renal MRI was performed one day before IRE for current tumour measurement and pretreatment planning (see Pretreatment planning) [17]. Due to the protocol, required tumour biopsy prior to ablation could precede IRE as initial diagnosis for histological proof of RCC in uncertain imaging or in the same session using the general anaesthesia required for IRE in obvious malignant imaging [1, 17].

Before IRE treatment, CT-guided coaxial core biopsies were taken from all tumours for initial histological assessment (case 1-3 with delay between). For IRE treatment, we used the NanoKnife™ IRE electroporator (AngioDynamics Inc.,® USA; firmware V3.29, software V2.2.0.23) and NanoKnife™ monopolar probes (15 cm, 19G). The electrodes were positioned under CT guidance (Aquillion prime CT scanner, Toshiba Inc.,® USA) and on the basis of individual treatment-planning data (ProcedureManager-2_2_0_23 for Windows, AngioDynamics®). IRE was performed with ECG triggering, under general anaesthesia and deep muscle paralysis. After 28 days, open partial kidney resection or radical nephrectomy with complete resection of the ablation region was performed [1]. To identify the spatial position of the resectate or tumour for the resection, the resectate will be anatomically land-marked intraoperatively with threads, as is usual. Renal MRI was performed one day before IRE.

The patient and treatment parameters are shown in Table 1. Intraprocedural modification was performed after immediately evaluation of post-IRE ablation graphs by interelectrode voltage modulation and separate electrode pair ablation. A complete ablation was defined as end-point with following characteristics: at least a complete ablation per electrode pair; simulated complete coverage of the tumour (target zone) by the treatment-planning zone; ideal (typically configurated) IRE ablation pulse graphs according to the manual [18]. The evaluation of the graphs was performed immediately after each pulse train application by at least two IRE experienced urologists and two IRE experienced interventional radiologists on the NanoKnife generator display.

Histopathological Analysis

Pre-IRE tumour biopsy specimens were fixed in 4 % buffered formalin, paraffin embedded, cut at 3 µm and stained with haematoxylin and eosin (HE). The resection specimens were fixed in buffered 4 % formaldehyde solution for at least 24 h followed by complete sectioning of the ablation area including a border of macroscopically inconspicuous kidney tissue in 0.4-cm-thick slices [19]. The ablation area was measured two dimensionally. In the case of nephrectomy, coarse sectioning of the remaining preparation was performed to exclude other pathologies. Thereafter, the ablation area, including the border, was completely embedded in paraffin in standard tissue cassettes after topographic assignment based on

Table 1 Patient and treatment parameters according to the Standardization of Terminology and Reporting Criteria for Image-Guided Tumor Ablation [21, 31]

	Patient 1 (44 years)	Patient 2 (78 years)	Patient 3 (74 years)
Tumour data			
No. targets	1	1	1
Tumour location	Upper pole, right, cortical, exophytic, ventrolateral	Upper to mid-pole region, right, cortical, exophytic, dorsomedial	Upper to mid-pole region, right, cortical, exophytic, dorsomedial, close to hilus
Tumour size (cm)	1.7 × 1.7 × 1.6	1.5 × 1.5 × 1.4	1.6 × 1.5 × 1.5
Tumour volume (ccm)	2.4	1.6	1.9
Tumour shape and class	Spherical, small	Spherical, small	Spherical, small
Biopsy	Pap RCC Typ 1, Fuhrman G2	Eosinophils cc RCC, Fuhrman G1	cc RCC, Fuhrman G1
Tumour texture	Inhomogeneous, solid, no cysts/calcification	Inhomogeneous, solid, no cysts/calcification	Inhomogeneous, solid, no cysts/calcification
TNM	pT1a G2 (C3)	pT1a G1 (C3)	pT1a G1 (C3)
	cN0 cM0 (C2) stage I	cN0 cM0 (C2) stage I	cN0 cM0 (C2) stage I
IRE parameter			
Procedures/sessions	1	1	1
Electrode type	Monopolar	Monopolar	Monopolar
No. of electrodes	4	3	4
No. of ablation pairs	6	3	6
Tip exposure[a] (cm)	2.5	1.5	2.0
Electrode configuration	Square	Triangular	Square
Interelectrode spaces (cm)	edge: 0.9–1.1, diagonal: 1.3–1.5	edge: 1.0–1.3; diagonal: n.a.	edge: 1.4–2.3, diagonal: 1.4–1.7
Ablation margin (cm)	0.2–0.6	0.3–0.5	0.5–1.4
Treatment zone (cm)	2.4 × 2.9 × 3.5[a]	2.5 × 2.5 × 2.5[a]	3.5 × 4.0 × 3.0[a]
Treatment zone (ccm)	12.7	8.2	22.0
No. of ablations	4 (plus 1 test run)	2 (plus 1 test run)	3 (plus 1 test run)
Pulse length	90 µs	90 µs	90 µs
Total no. of pulses	1300	450	1320
Current (max.)	49 A	42 A	49 A
Voltage (min./max.)	1800/2800 V	2200/2640 V	1960/3000 V
Surgery			
Resection type	Partial kidney resection	Partial kidney resection	Radical nephrectomy
ypTNM	ypT1a V0 L0 Pn0 R0 (C4)	ypT0 V0 L0 Pn0 R0 (C4)	ypT0 V0 L0 Pn0 R0 (C4)

Tumour and ablation volume ($V = \frac{1}{6}\pi d^3$, respectively, $\frac{4}{3}\pi abc$)

[a] Active tip (exposure) plus postulated ablation field in depth 2 × 0.5 cm [18]

macrophotography. Each tissue block was used to prepare 3-µm-thick sections, and these were stained with HE for morphological assessment in 500 µm steps with one unstained section each for transmission microscopy. Additional immunohistological staining of the tumour region with proliferation marker Mib1 (Dako; dilution 1:100) at least still rudimentary basic structure was performed to determine viability or irreversible cell death.

In each specimen, the complete ablation area, the tumour area and non-affected renal tissue on each slide was precisely outlined in multicoloured ink. The maps from each subject were computer scanned, inspected serially and determined by a digitising pad (Bamboo One™) and image-manipulation software (GIMP 2.8.14®). Volume was calculated as the sum of tumour areas multiplied by the section thickness (0.4 cm) and by a formalin-induced tissue-shrinkage factor of 1.5.

The extent of histologically demonstrable damage was determined by examining the histostructural changes (disorganisation of the original tumour structure) and also the cellular changes (ballooning, vacuolisation and nuclear pyknosis), and a regression grade (RG) was assigned according to the scale shown in Table 2 [19, 20].

Table 2 Histological-cellular grading of the regressive alterations of the RCC after IRE, adapted from Ref. [20]

RG	Histological and cellular morphology
0	No regression: Neither necrosis nor cellular or structural alterations
1	Slight regression: necrosis or disappearance of the tumour and/or cellular or structural alterations in less than 1/3 of the tumour
2	Moderate regression: necrosis or disappearance of the tumour and/or cellular or structural alterations in more than 1/3, but not more than 2/3, of the tumour
3	Strong regression: necrosis or disappearance of the tumour and/or cellular of structural alterations in more than 2/3 of the tumour, but still histomorphologically intact or only slightly altered tumour cells distinguishable
4	Complete regression: tumour completely necrotic and/or replaced by fibrosis. No histomorphologically intact tumour cells distinguishable

DR degree of regression

Results

Case 1 (Fig. 1)

Initial biopsy Initial biopsy revealed papillary RCC of type 1 (Fig. 1D). *Treatment* partial kidney resection. *Macroscopic analysis* Sharply demarcated, approximately ellipsoidal, haemorrhagically altered ablation zone. In the centre of the ablation zone, a round to oval tumour focus was clearly delineated. The greatest width of the peritumoural damage zone was 8 mm, spreading to peritumoural renal tissue and to perirenal fatty tissue (Fig. 1E, F–K). *Microscopic analysis* The tumour focus within the ablation zone showed strong treatment effects (RG III) with almost complete tumour destruction by extended, homogeneously eosinophilic coagulation necrosis (Fig. 1L). Within the necrotic tumour only, a small focus of preserved residual papillary tumour, comprising 18.7 % of the posttreatment tumour zone (12 % of the pretreatment tumour zone), was detected. The residue showed only minor regressive changes without demonstrable proliferative activity (Fig. 1L, O; Tables 2, 3; regression grade 3).

Case 2 (Fig. 2)

Initial biopsy Equivocal oncocytic renal tumour. On account of its staining profile (CD 10+, Vimentin−, cytokeratin 20−, Hale–) classified as clear-cell RCC of the eosinophilic subtype (Fig. 2D). *Treatment* partial kidney resection. *Macroscopic analysis* sharply demarcated, semi-ellipsoidal ablation zone with a broad base at the kidney surface and ellipsoidal intrarenal extension. At the ellipsoidal end clearly demarcated tumour focus. Extensive signs of local haemorrhage. Peritumourally a narrow (1 mm) margin of haemorrhagic surrounding tissue. A 9 mm margin to the kidney surface was present (Fig. 2E, F–I). *Microscopic analysis* The tumour focus within the ablation zone showed extensive coagulation necrosis with intratumoural haemorrhage, partly fresh and partly older as well as focal granulation tissue formation. Within the necrotic tumour, a small tumour focus comprising 2.8 % of the pre- and posttreatment tumour zone with rudimentary preserved histoarchitecture was seen (Fig. 2F–I). This focus showed severe cytological damage (homogeneous cytoplasm eosinophilia, cell hydropsy, cell-wall destruction with only schematically distinguishable cell nuclei and loss of nucleoli) without signs of proliferative activity in Mib-1 staining. The regressive changes were graded as RG 4 (Fig. 2J–L; Tables 2, 3).

Case 3 (Fig. 3)

Initial biopsy Clear-cell RCC (Fig. 3C). *Treatment* radical nephrectomy due to intraoperative findings (severe inflammatoric and fibrotic perifocal reaction with involvement of the hilus) (Fig. 4). *Macroscopic analysis* Extended geographic ablation zone with a central capsule-like, delimited tumour focus (Fig. 3E–L). Far-reaching peritumoural extension of the ablation region (width up to 11 mm) to the renal cortex and medulla, associated vessel structures, renal pelvis and perirenal fat (Fig. 5). *Microscopic analysis* The tumour focus within the ablation zone showed strong treatment effects (RG 4) with formation of extended homogeneous, acellular, eosinophilic coagulation necrosis and inclusion of an area with rudimentary preserved histoarchitecture (62.4 % of the preatreatment tumour zone resp. 91.2 % of the posttreatment tumour zone) which showed massive cytological damage (RG 4) without sign of a residual proliferative activity (Fig. 3M–O; Tables 2, 3).

Volumetry, Histological Planimetry and Volumetry

See Table 3 and Fig. 4

Zonal Histological Structuring of the Ablation Zone

Alongside the case-specific tumour-related histological changes described above, all cases showed a zonal structuring of the ablation region. In the centre, an amorphous necrosis zone of the coagulation-necrosis type (zone Z1 in Fig. 5A, B) was seen [21]. Next to this, there was a

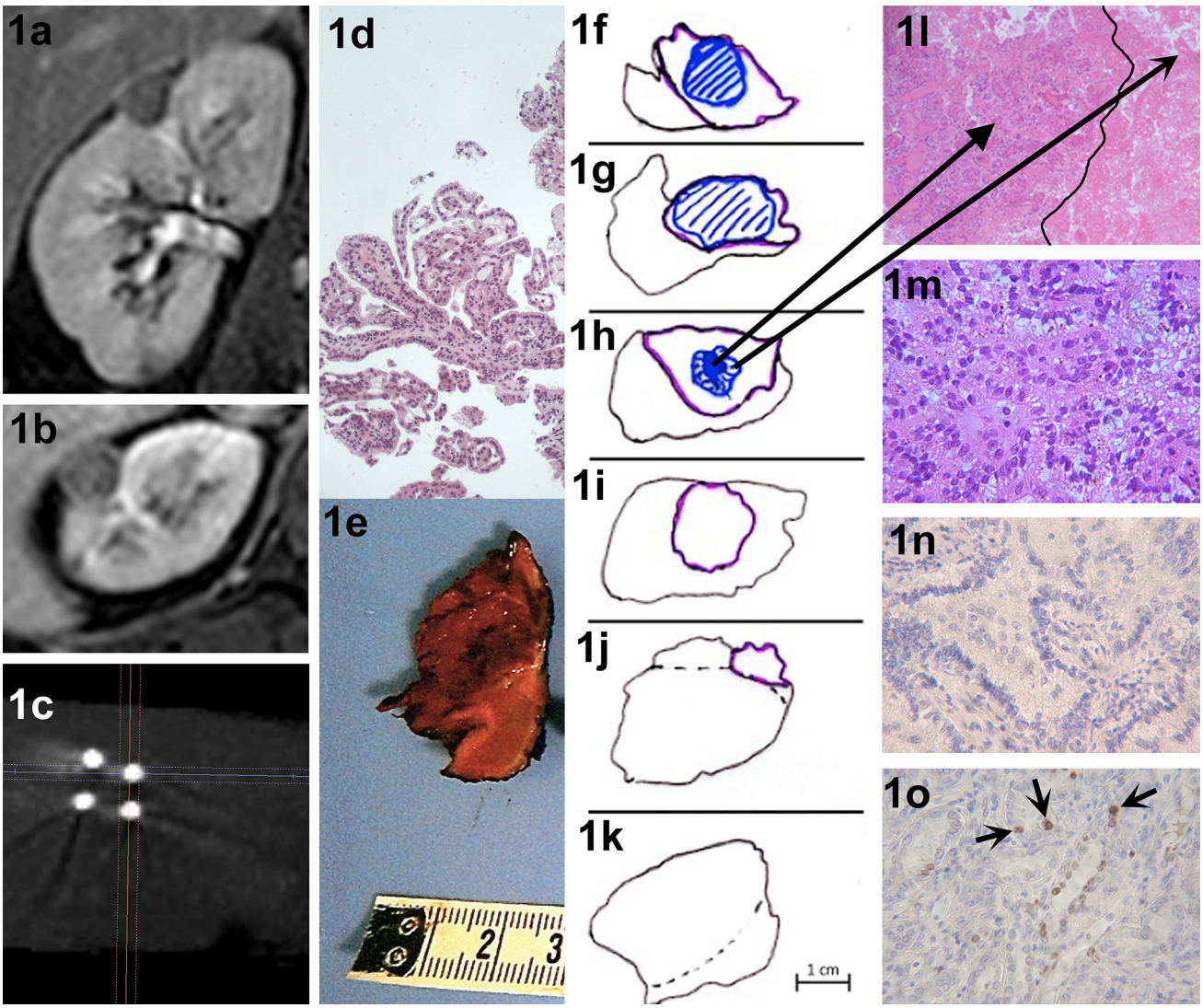

Fig. 1 Case 1: **A**, **B** Pre-interventional MRI coronal/transverse. **C** Check of IRE electrode placing in CT. **D** Histology of initial biopsy showing type 1 papillary RCC. **E** Macroscopic view of renal specimen with sharply demarcated ablation zone. **F–K** Macro- and microscopic fusion sketch of the serially sectioned renal specimen (**F** sketch corresponding to **E**): *violet line* ablation zone (including zone 2 and 3 as shown in Fig. 5), *blue-hatched area* tumour zone, *solid blue area* part of tumour zone with preserved histo- and cytoarchitecture; *black dashed line* border to perirenal fat. **L** Papillary NCC after IRE: ablated tumour area with complete necrosis of coagulation type on the *right of the black line* (corresponding to the *blue-hatched area* in the fusion sketches). Sharply adjacent tumour area with partially preserved histo- and cytomorphology on the *left of the black line* (corresponding to the *solid blue area* in the fusion sketch, haematoxylin–eosin (HE) staining) **M** Histologic detail view of the preserved tumour region from **L** showing papillary architecture and minor signs of cytologic damage (cell hydrops, cytoplasmic vacuolization, isolated pycnotic nuclei) (HE). **N** Same tumour area as in 1 m with negative staining for the proliferation marker Mib-1. **O** Low proliferative activity (individual nuclear-stained cells, *arrows*) of normal renal cortex tissue distant from the lesion (Mib-1 immunohistochemistry)

necrosis zone of variable width, also of the coagulation-necrosis type, in which ghost structures of the tissue affected could still be discerned (e.g., tubuli, glomeruli, fat; zone Z2 in Fig. 5A, C). Some dystrophic areas of calcification and resorptive chronic-inflammatory changes could also be seen, sometimes with the formation of foreign-body giant cells. In sections where the ablation zone included the renal pelvis and papillae, both structures showed necrosis with urothelial sloughing. Adjacent to this zone, there was a gradual transition to a zone of granulation tissue (zone Z3) with a width between 1 to 5 mm (mean 2.45 mm, data not shown). Zone 3 was associated with frequent, in part luminal occlusive intimal hyperplasia of small- and medium-sized arterial renal vessels. Adjacent to this, unaffected renal parenchyma (urp) was found (unaffected renal parenchyma = URP, Fig. 5A, D–F).

Table 3 Volumetry, histological planimetry, degree of regression, residual vitality

	Case 1	Case 2	Case 3
Pretreatment (planning, MRI)			
Tumour size (target size) (cm)	1.7 × 1.7 × 1.6	1.5 × 1.5 × 1.4	1.6 × 1.5 × 1.5
Volume tumour (ccm)	2.4	1.6	1.9
Treatment zone (cm)	2.4 × 2.9 × 3.5[#]	2.5 × 2.5 × 2.5[#]	3.5 × 4.0 × 3.0[#]
Volume treatment (planning) zone (ccm)	12.7	8.2	22.0
Posttreatment (histological)			
Tumour size (cm)	1.6 × 1.5 × 1.2	1.6 × 1.7 × 1.1	1.5 × 1.4 × 1.2
Volume treated tumour (contour) (ccm)	1.5	1.6	1.3
Volume residual tumour (ccm)	0.28	0.045	1.185
Ablation zone[a] size (cm)	2.5 × 2.0 × 1.3	3.0 × 2.5 × 2.0	4.2 × 3.0 × 2.6
Ablation zone[a] volume (ccm)	3.4	7.9	17.2
Tumour characteristics			
RCC type	Papillary	Clear cell	Clear cell
Regression grade (Table 2)	3	4	4
Residual tumour of pretreatment tumour size (%)	12	2.8	62.4
Residual tumour of posttreatment tumour size (%)	18.7	2.8	91.2
Mib-1 labelling index (%)[b]	0	0	0
Assessment of viability	Uncertain	Non-viable	Non-viable
Post–Pre-IRE proportions			
Δ Tumour volume (involution/shrinkage) (ccm)	−0.9	0	−0.6
Δ Tumour volume (involution/shrinkage) (%)	−37.5	0	−31.6
Δ Volume Ablation zone[a]—treatment (plan.) zone (ccm)	−9.3	−0.3	−4.8
Q Volume ablation zone[a]/treatment (plan.) zone (%)	+26.8	+96.3	+79.2

Treated tumour is residual visible tumour shape (volume) with histological signs of posttreatment alteration of the complete tumour area. Residual tumour is histologically residual tumour structure without signs of complete destruction

Volume ($V = \frac{1}{6}\pi d^3$, respectively, $\frac{4}{3}\pi abc$)

[a] Ablation zone includes zone Z2 and Z3 as defined in Fig. 5

[b] Percentage of Mib-1-nuclear-labelled tumour cells

Discussion

This pilot study is intended to assess the results obtained from resection after curative IRE of localised RCC in humans. This allows a first-ever clinical check of the hitherto mostly pre-clinical considerations of the general mechanism, the non-thermal ablation characteristics and the organ-independent effectiveness of IRE. In this preliminary interim analysis, the following hypotheses were considered: Early experiments had shown a shrunk scarring 2–4 weeks after apoptosis induction by IRE, assuming macrophagocytic degeneration of the ablation zone. A concentric-zonal character of the ablation zone has been described [7]. In contrast to this, monitoring of IRE-induced ablation exclusively by imaging and biopsy (for various types of tumour) revealed persistent tumour structures [15]. Assuming that the effect of IRE is non-thermal, this leads to the hypothesis that one must reckon with the continued presence of regressively altered tumour cells, dependent upon the time that has elapsed since IRE. The assessment of viability of these cells is particularly important. The required regression grading of RCC after non-operative treatment does not yet exist and would have to be established for progress-monitoring by biopsy (see e.g. Table 2) [1, 19]. The best time for this assessment must also be established. On the basis of the resection results (ablation and tumour geometry), the study parameters would also require adjustment.

Zonal Structuring of the Ablation Zone

The histological analysis of the tumour specimens confirmed a zonal structuring of the ablation zone as already described in previous animal studies [7, 10, 11]. A conspicuous feature was the detection of a central necrotic region in all of our cases. This largely unreactive

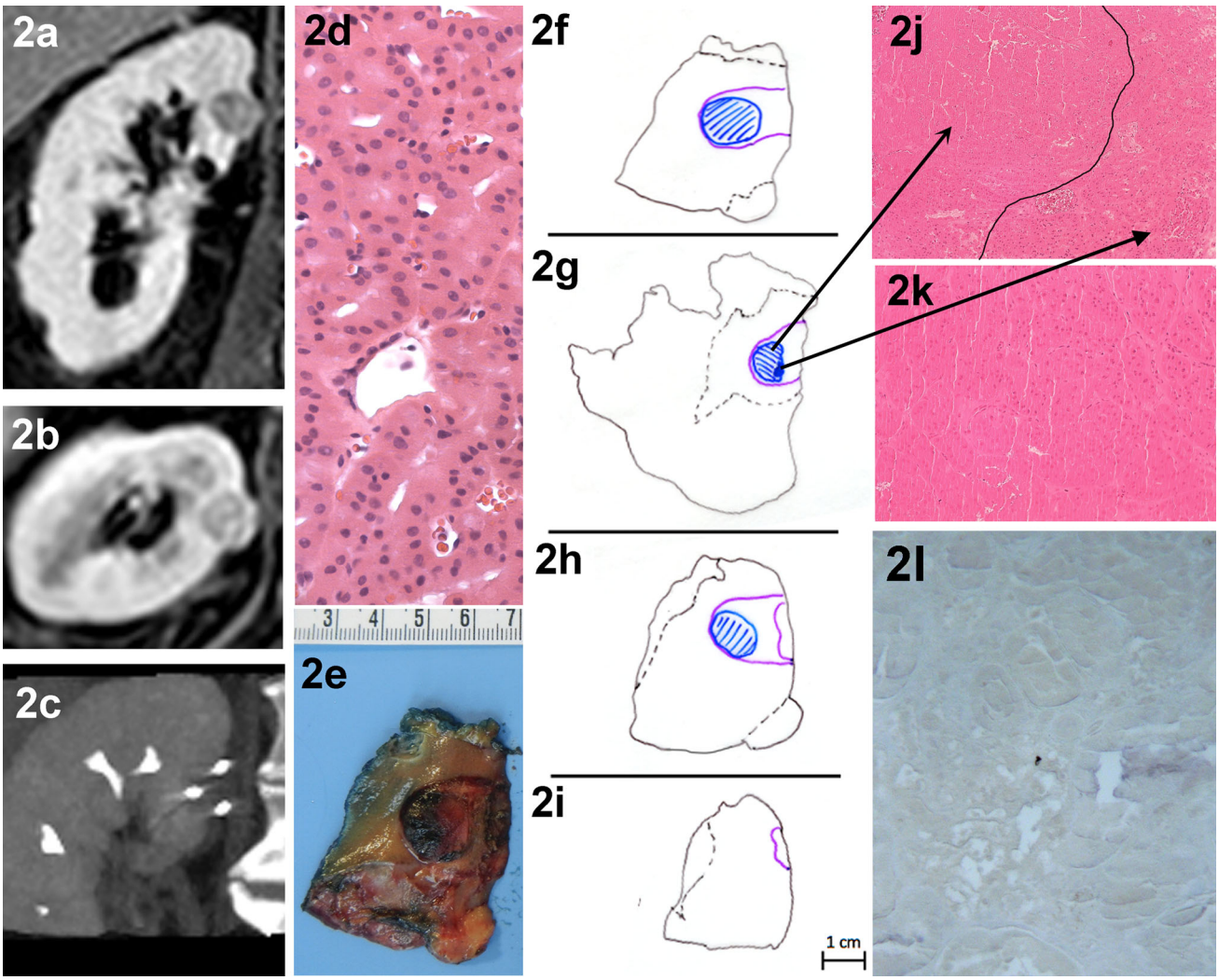

Fig. 2 Case 2: **A**, **B** Pre-interventional MRI coronal/transverse. **C** Check of IRE electrode placing in CT after administration of contrast enhancer. **D** Histology of initial biopsy showing ccRCC of eosinophilic subtype. **E** Macroscopic view of renal specimen with ablation zone. **F**–**I** Macro- and microscopic fusion sketch of the sectioned tumour resectate (sketch **F** corresponding to Fig. 2E): *violet line* ablation zone (including zone 2 and 3 as shown in Fig. 5), *blue-hatched area* tumour zone, *solid blue area* part of tumour zone with rudimentary preserved histo- and cytoarchitecture, *black dashed line* border to perirenal fat. **J** ccRCC after IRE: ablated tumour area with complete necrosis of coagulation type on the *left of the black line* (corresponding to the *blue-hatched area* in the fusion sketches). Sharply adjacent tumour area with hardly recognizable residual histoarchitecture on the *right of the black line* (corresponding to the *solid blue area* in the fusion sketch, haematoxylin-eosin (HE) staining*). **K** Detail view of tumour necrosis with rudimantory tumour architecture and severe signs of cytological damage (destroyed cell walls, cell hydrops, shadow nuclei, (HE)). **L** Same tumour area as shown in **K** with negative staining for the proliferation marker Mib-1

coagulation/infarction necrosis made up the greatest part of the damage zone (zone 1). To date, only one previous study [7] reported on a damage pattern of this kind of limited extend 28 days after IRE, which corresponds to the age of zone 1 in the current study (Figs. 1, 2, 3, 5).

Considering further its size, homogeneity, damage pattern as well as its sharp delineation suggests that zone 1 corresponds to the initial damage zone of IRE (Fig. 5A). In contrast to the finding of initial pre-clinical studies [7], this zone 1 did not pass directly over into normal surrounding tissue. Rather, it was surrounded by two further zones of damage (zones 2 and 3, Fig. 5). The histological picture of zone 2 suggests more recent damage, about 7 days old. One must therefore proceed on the assumption of a two-phase process. In subsequent studies with a defined interval between IRE and resection, it will be necessary to take into account whether, and if so when, this secondary tissue damage increases the initial ablation volume.

Zones 2 and 3 might have their origin in one or both of the following mechanisms:

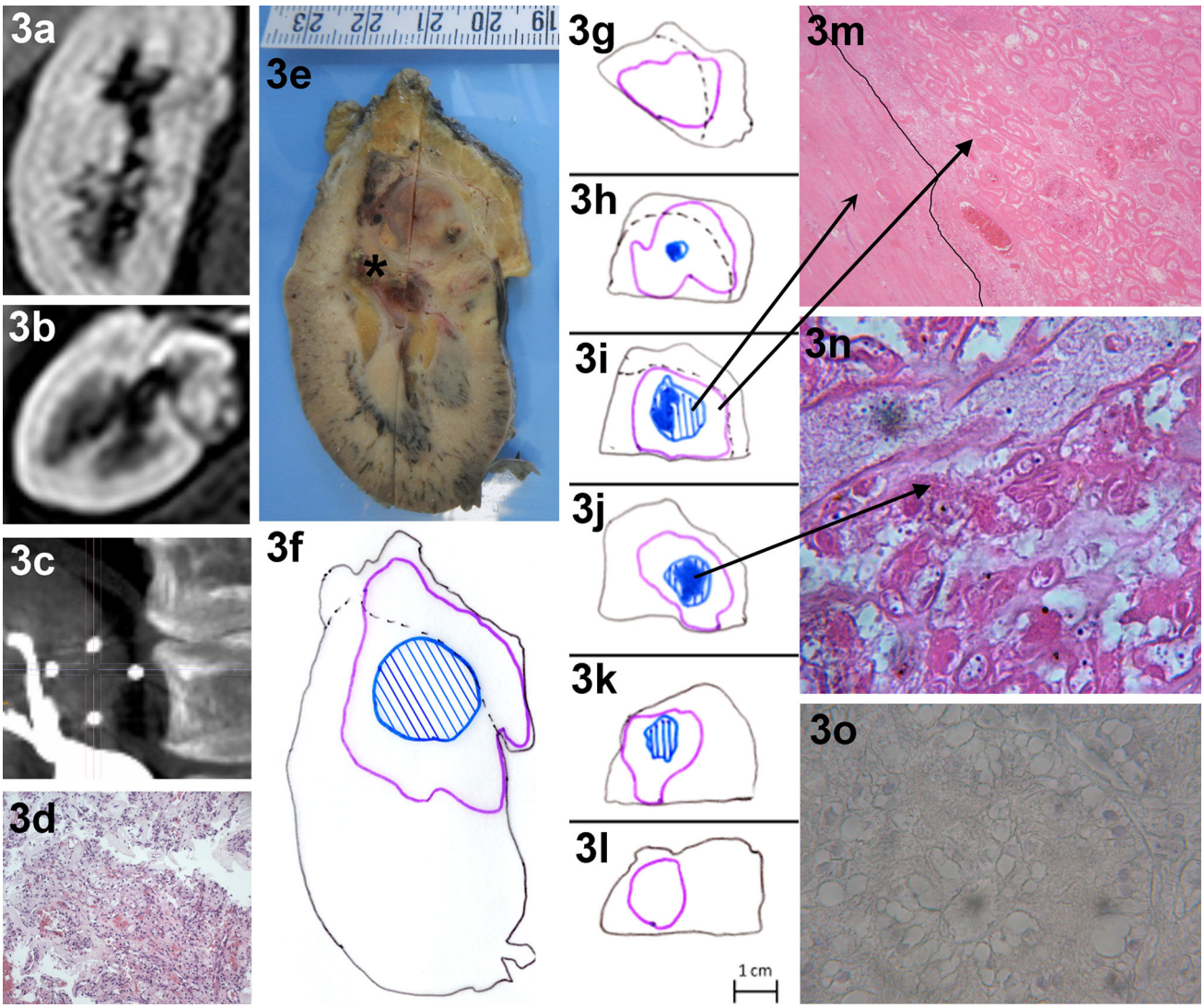

Fig. 3 Case 3: **A**, **B** Pre-interventional MRI coronal/transverse. **C** Check of IRE electrode placing in CT. **D** Histology of initial biopsy showing ccRCC. **E** Macroscopic section of the nephrectomy preparation with ablation region, which covers ca. 2/3 of the cranial kidney region; renal pelvis (*). **F** Macro- and microscopic fusion sketch of the nephrectomy specimen (corresponding to **E**), **G**–**L**: sketches of serially sectioned tumour bearing ablation zone. For all sketches: *violet line* ablation zone (including zone 2 and 3 as shown in Fig. 5), *blue-hatched area* tumour zone, *solid blue area* part of tumour zone with still distinguishable histo- and cytoarchitecture; *black dashed line* border to perirenal fat. **M** Ablated tumour area with complete coagulation necrosis on the *left of the black line* and a sharp transition to the bordering non-tumour parenchyma with less homogeneous coagulation necrosis showing contours of necrotic tubuli on the *right of the dashed line* (HE). **N** Necrotic tumour portion with still recognisable basis structure and signs of severe cytological damage (destroyed cell walls, cytoplasm vacuolisation and nuclear destruction; HE). **O** The absence of detection of proliferative activity (nuclear negativity) of the tumour section from 3n (Mib-1 immunohistochemistry)

– The energy of the electric field decays "centrifugally". A lower voltage gradient—below the postulated lower efficacy limit for IRE—explains the sharp primary demarcation of the ablation region. Histological transformation processes in the ablation region (cell clusters, interstitial processes, capillaries) could lead to secondary, nutritive damage (diffusional changes) by perturbation of cellular homeostasis in the immediately adjacent tissue.

– Zones 2 and 3 show conspicuous vascular alterations. The intralobar arteries show prominent mural thickening, in part with complete luminal obliteration (Fig. 5E, F). This phenomenon is of interest as it was seen clearly, in all cases, in the region of zones 2 and 3. This kind of vessel damage has been described in animal experiments [7]. Hypoxic effects caused by the initial tissue damage is known to induce vascular intima hyperplasia—up to complete obliteration of

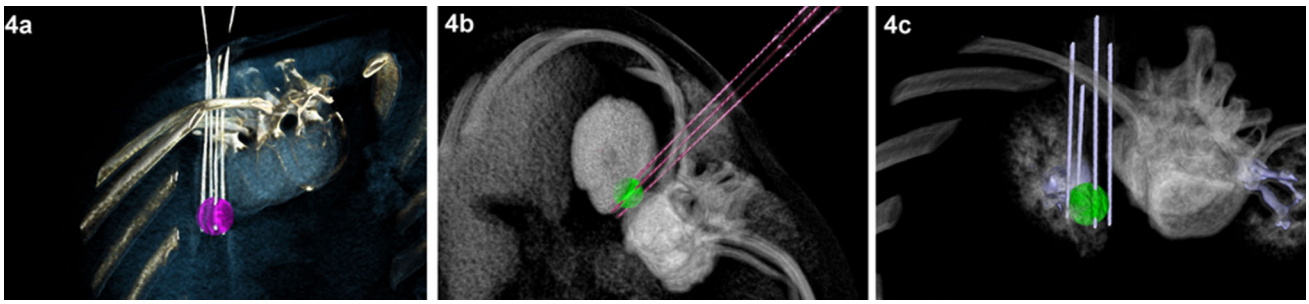

Fig. 4 3D-CT-reconstruction of the IRE electrode placing (case 1, **A**; case 2, **B**; case 3, **C**)

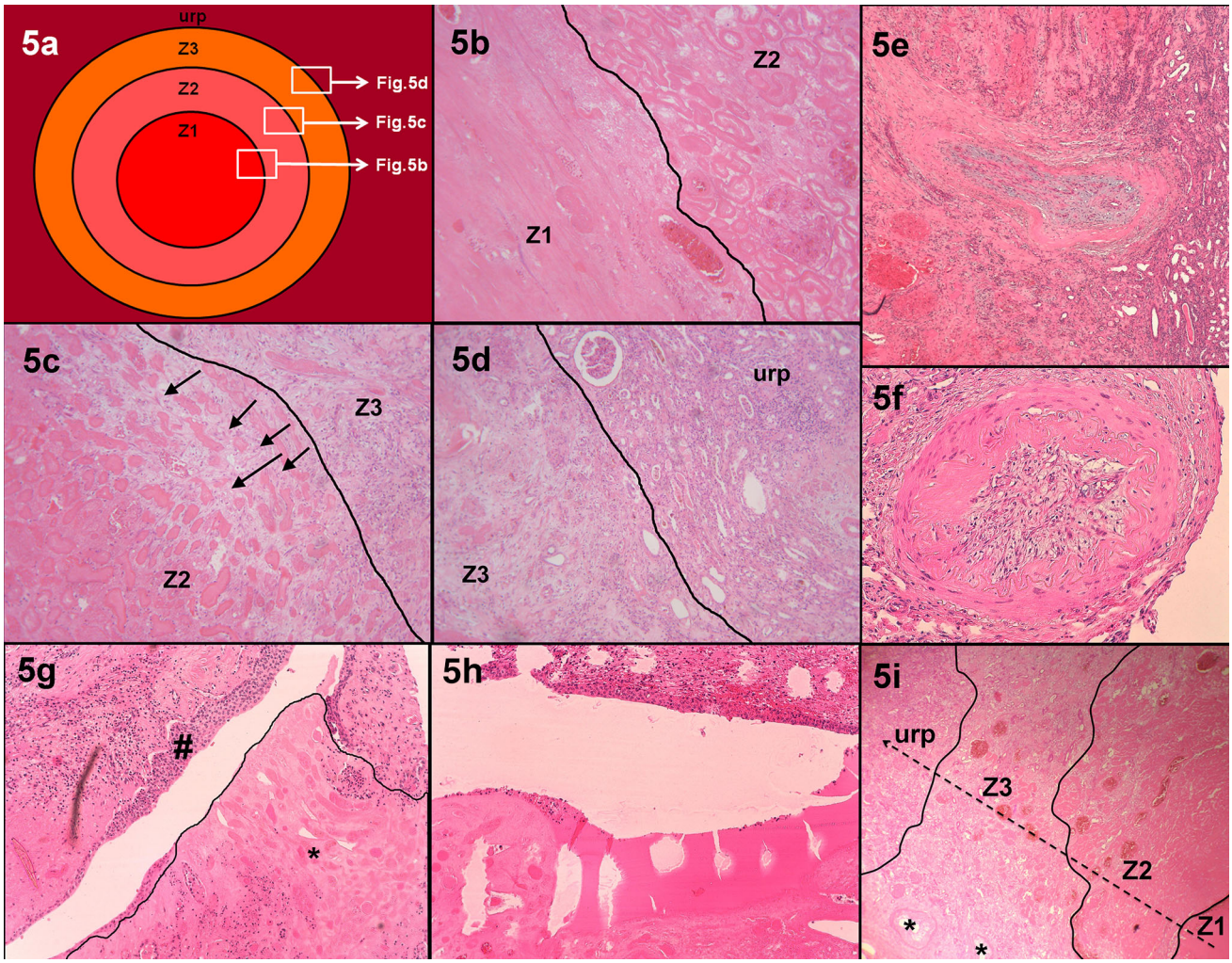

Fig. 5 **A** Macroscopic/microscopic structural sketch of the ablation region with trizonal structuring of tissue damage. **B** Damage zone Z1 of the type amorphous-coagulation necrosis, passing over into damage zone Z2, also of the type amorphous-coagulation necrosis but with discernable basic tissue structure. **C** Zone Z2, at the periphery, with sprouting by connective tissue (*arrows*) and, adjacent to this, transition to damage zone Z3, which consists of a fibrosis seam with formation of granulations tissue. **D** Transition from zone Z3 to unaffected renal parenchyma (urp). **E** Zone 3 arterial vessel with vaso-occlusive intima hyperplasia. **F** Detail of a zone 3 small arterial vessel with vaso-occlusive intima hyperplasia. (**B**–**F**: HE staining). **G** Treatment effect on renal pyelon showing necrotic renal papilla* covered by partially necrotic urothelium with urothelial sloughing. # non-affected intact urothelium. Yet no signs of stricture formation or luminal obliteration. **H** Histologic details from **G**. **I** low power microphotograph showing the zonal distribution of the ablation zone (Z1–Z3) as described above. * zone 3 vessels with prominent intima proliferation

surrounding vessels which could lead to ischaemia-based secondary necrosis. The origin of this might lie in the vascular-lock phenomenon described above [3, 9, 22, 23].

Volumetry

The ablation volumes found by histology corresponded to the planned ablation volumes in that in each case the actual ablation volume (zone 1–3) completely included the tumour volume. In the histological volumetry the reduction in tumour volume (delta post-minus pretreatment tumour volume) was −37.5 %, 0 % and −31.6 % for cases 1, 2 and 3, respectively. The proportion of in ablation versus treatment (planning) zone/volume (quotient) was 26.8, 96.3 and 79.2 % for cases 1, 2 and 3, respectively. The differences (pre–post) in both ablation and tumour volumes are best explained by a combination of shrinkage induced by IRE (tissue remodelling), by resection (lack of perfusion) and by formalin fixation.

On the basis of the very small number of patients investigated so far, no meaningful statistical assessment is possible. However, it already appears that a parallel shrinkage of both volumes takes place. The secondary necrosis could also possibly have a quantitative influence on this tissue shrinkage (Fig. 5). To what extent the region of secondary necrosis in zones 2 and 3 (Fig. 5) exceeds the area of the primary ablation field cannot at present be decided, on account of the shrinkage of the ablation region and the difficulty in calculating it. However, this is probably not relevant in clinical application, because of the inherent inaccuracy of 1–2 mm in the CT-guided placing of the IRE electrodes, even with layer thicknesses of 1 mm (Fig. 4). Because of the tissue remodelling after 28 days (involution), and shrinkage due to formalin fixation, an exact correlation of the observed ablation volumes to the planned treatment volumes is not possible. However, the goal of completely coveraging the tumour area by the ablation zone was achieved while at the same time the kidney was preserved.

Summary of Tumour Histopathology

In this study, histologically altered tumour structures were observed after an interval of 4 weeks between IRE and resection; these showed various degrees of change. To assess these findings systematically, we used an adapted regression grading (Table 2). These histologies represented "snapshots" 4 weeks after IRE, with specific findings. Although the choice of a different interval between IRE and histological analysis could of course influence this result, the optimum interval between IRE and histological assessment is at present still unclear.

In each of the three cases investigated, IRE-induced massive damage to the tumour tissue. In no case did a tumour residue appear at the edge of the ablation zones. The minimum safety margin was ca. 1 mm (medullary), and the greatest margin was 8–11 mm (cortical), on account of the tumour's position.

The tumour damage comprised complete tumour necrosis in cases 2 and 3, while in case 1 almost complete tumour necrosis was observed, with a residual tumour that measured 8 mm and made up 12 % of the original tumour volume; according to Mib-1 staining, it had no proliferative activity (Case 1). However, Mib-1 immunohistochemistry is only of limited in assessing the viability of slowly proliferating tumours such as RCC, especially of small residues comprising only few cells. Therefore, a residual viability cannot be excluded with certainty on a histological basis, in spite of the negative immunohistochemical reaction to the proliferation marker Mib-1. The assessment of apoptosis or programmed cell death by the terminal transferase-mediated nick end labelling technique represents an additional technique of tissue viability testing. Due to well-known technical pitfalls [24], we initially decided to abstain from TUNEL staining. However, due to the remaining uncertainty concerning residual tumour viability, we will apply TUNEL staining in future investigations.

It is also unclear whether, the massive perifocal structure and vessel damage would here also have led to complete necrosis of this tumour region. It remains uncertain as to whether the basic histological structure of this tumour residue (papillary RCC) and/or a non-optimised IRE field was the cause of this [25, 26].

At least the meta-analyses of patients with positive surgical margin after nephron-sparing surgery of RCC suggests a lack of prognostic relevance of small tumour residues. Therefore, a surveillance strategy seems preferable to surgical reintervention [27, 28]. Small, dubious tumour residues remaining in the non-viable ablation region 4 weeks after IRE must be assessed in the light of this. Similarly, residual tumour areas are seen following RFA that possess a residual viability immediately and one week after ablation [29, 30]. Following IRE of liver tumours, for comparison, 29 % showed recurrent tumour after 6 months [25].

Conclusion

IRE (with used recommended clinical parameters in this treatment protocol) could be an effective treatment and led to near-total or total destruction of various histological RCC subtypes. 4 weeks after IRE, novel histological findings were made. The postulated homogeneous, isomorphic tissue damage by IRE could not be confirmed.

Instead of this, a new zonal distribution of IRE damage was described. The assessment of the viability and clinical relevance of very small amounts of residual tumour is difficult. Viable tumour cells may be possible within an IRE ablation zone. Up to that preliminary point an alteration of the ablation parameters cannot be recommended. Because of the tissue remodelling after 28 days (involution), and shrinkage due to formalin fixation, an exact correlation of the observed ablation volumes to the planned treatment volumes is not possible. However, at least, the goal of complete coverage of the tumour by ablation zone while focal ablation with preserving of the kidney was achieved. On the basis of various observables (depth of target, breathing movement, puncture window, manual CT-guided electrode placement), an ablation volume reduced to that of the renal tumour appears feasible (Fig. 4). According to these initial, preliminary study results of the first three renal cases, the curative intended, renal saving focal ablation of localised RCC below <3 cm by percutaneous IRE by the NanoKnife system appears to be possible but needs further, systematic evaluation for optimation of this treatment method and treatment protocol.

Compliance with Ethical Standards

Conflict of Interest Author 10 (Martin Schostak) has received funding for conference attendance from AngioDynamics Inc. (New York, USA). Neither of these sources provided any input whatsoever into this article or this study. The other authors declare that they have no conflict of interest.

Ethical Approval All procedures performed in studies involving human participants were in accordance with the ethical standards of the institutional and/or national research committee and with the 1964 Helsinki declaration and its later amendments or comparable ethical standards.

Informed Consent Informed consent was obtained from all individual participants included in this study. Additional informed consent for identifying information does not apply.

References

1. Ljungberg B, Bensalah K, Bex A, Canfield S, Dabestani S, Hofmann F, Hora M, Kuczyk MA, Lam T, Marconi L, Merseburger AS, Mulders PFA, Powles T, Staehler M, Volpe A. EAU guidelines on renal cell carcinoma. http://uroweb.org/guideline/renal-cell-carcinoma/#. Accessed 26 April 2015.
2. Castro A Jr, Jenkins LC, Salas N, Lorber G, Leveillee RJ. Ablative therapies for small renal tumours. Nat Rev Urol. 2013;10(5):284–91. doi:10.1038/nrurol.2013.68.
3. Rubinsky B. Irreversible electroporation. 1st ed. Berlin: Springer; 2009. p. 328. ISBN 3642054196.
4. Silk M, Tahour D, Srimathveeravalli G, Solomon SB, Thornton RH. The state of irreversible electroporation in interventional oncology. Semin Intervent Radiol. 2014;31(2):111–7. doi:10.1055/s-0034-1373785.
5. Sommer CM, Fritz S, Wachter MF, Vollherbst D, Stampfl U, Bellemann N, Gockner T, Mokry T, Gnutzmann D, Schmitz A, Knapp J, Longerich T, Kuhn-Neureuther C, Pereira PL, Kauczor HU, Werner J, Radeleff BA. Irreversible electroporation of the pig kidney with involvement of the renal pelvis: technical aspects, clinical outcome, and three-dimensional CT rendering for assessment of the treatment zone. J Vasc Interv Radiol. 2013;24(12):1888–97. doi:10.1016/j.jvir.2013.08.014.
6. Olweny EO, Kapur P, Tan YK, Park SK, Adibi M, Cadeddu JA. Irreversible electroporation: evaluation of nonthermal and thermal ablative capabilities in the porcine kidney. Urology. 2013;81(3):679–84. doi:10.1016/j.urology.2012.11.026.
7. Wendler JJ, Porsch M, Hühne S, Baumunk D, Buhtz P, Fischbach F, Pech M, Mahnkopf D, Kropf S, Roessner A, Ricke J, Schostak M, Liehr UB. Short- and mid-term effects of irreversible electroporation on normal renal tissue: an animal model. Cardiovasc Intervent Radiol. 2013;36(2):512–20. doi:10.1007/s00270-012-0452-7.
8. Wendler JJ, Pech M, Porsch M, Janitzky A, Fischbach F, Buhtz P, Vogler K, Hühne S, Borucki K, Strang C, Mahnkopf D, Ricke J, Liehr UB. Urinary tract effects after multifocal nonthermal irreversible electroporation of the kidney: acute and chronic monitoring by magnetic resonance imaging, intravenous urography and urinary cytology. Cardiovasc Intervent Radiol. 2012;35(4):921–6. doi:10.1007/s00270-011-0257-0.
9. Wendler JJ, Pech M, Blaschke S, Porsch M, Janitzky A, Ulrich M, Dudeck O, Ricke J, Liehr UB. Angiography in the isolated perfused kidney: radiological evaluation of vascular protection in tissue ablation by nonthermal irreversible electroporation. Cardiovasc Intervent Radiol. 2012;35(2):383–90. doi:10.1007/s00270-011-0187-x.
10. Deodhar A, Monette S, Single GW Jr, Hamilton WC Jr, Thornton R, Maybody M, Coleman JA, Solomon SB. Renal tissue ablation with irreversible electroporation: preliminary results in a porcine model. Urology. 2011;77(3):754–60. doi:10.1016/j.urology.2010.08.036.
11. Tracy CR, Kabbani W, Cadeddu JA. Irreversible electroporation (IRE): a novel method for renal tissue ablation. BJU Int. 2011;107(12):1982–7. doi:10.1111/j.1464-410X.2010.09797.x.
12. Liehr UB, Wendler JJ, Blaschke S, Porsch M, Janitzky A, Baumunk D, Pech M, Fischbach F, Schindele D, Grube C, Ricke J, Schostak M. Irreversible electroporation: the new generation of local ablation techniques for renal cell carcinoma. Urologe A. 2012;51(12):1728–34. doi:10.1007/s00120-012-3038-8.
13. Ball C, Thomson KR, Kavnoudias H. Irreversible electroporation: a new challenge in "out of operating theater" anesthesia. Anesth Analg. 2010;110(5):1305–9. doi:10.1213/ANE.0b013e3181d27b30.
14. Pech M, Janitzky A, Wendler JJ, Strang C, Blaschke S, Dudeck O, Ricke J, Liehr UB. Irreversible electroporation of renal cell carcinoma: a first-in-man phase I clinical study. Cardiovasc Intervent Radiol. 2011;34(1):132–8. doi:10.1007/s00270-010-9964-1.
15. Thomson KR, Cheung W, Ellis SJ, Federman D, Kavnoudias H, Loader-Oliver D, Roberts S, Evans P, Ball C, Haydon A. Investigation of the safety of irreversible electroporation in humans. J Vasc Interv Radiol. 2011;22(5):611–21. doi:10.1016/j.jvir.2010.12.014 **Epub 2011 Mar 25**.
16. Nielsen K, Scheffer HJ, Vieveen JM, van Tilborg AA, Meijer S, van Kuijk C, van den Tol MP, Meijerink MR, Bouwman RA. Anaesthetic management during open and percutaneous irreversible electroporation. Br J Anaesth. 2014;113(6):985–92. doi:10.1093/bja/aeu256.
17. Wendler JJ, Porsch M, Nitschke S, Köllermann J, Siedentopf S, Pech M, Fischbach F, Ricke J, Schostak M, Liehr UB. A prospective Phase 2a pilot study investigating focal percutaneous irreversible electroporation (IRE) ablation by NanoKnife in patients with localised renal cell carcinoma (RCC) with delayed interval tumour resection (IRENE trial). Contemp Clin Trials. 2015;43:10–9. doi:10.1016/j.cct.2015.05.002.

18. Manual NanoKnife® System Procedure & Trouble Shouting Guide. Software version 2.2.0. AngioDynamics®, © 2011 AngioDynamics, Inc. p. 1–159.
19. http://www.pathologie.de/fachinfos/nachschlagewerke-handbuchreihe/handbuch-leitlinien-pathologie/leitfaeden-detailansicht/?tx_ttnews%5Btt_news%5D=268&cHash=73875b5f47d3e8ac0b970cf6987ab03b.
20. Ninomiya Y, Yanagisawa A, Kato Y, Kitagawa T, Ishihara S, Nakajima T. Histological indications of a favorable prognosis with far-advanced gastric carcinomas after preoperative chemotherapy. J Cancer Res Clin Oncol. 1999;125(12):699–706.
21. DE Dupuy, Gervais DA, Gianfelice D, Gillams AR, Lee FT Jr, Leen E, Lencioni R, Littrup PJ, Livraghi T, Lu DS, McGahan JP, Meloni MF, Nikolic B, Pereira PL, Liang P, Rhim H, Rose SC, Salem R, Sofocleous CT, Sofocleous CT, Solomon SB, Soulen MC, Tanaka M, Vogl TJ, Wood BJ, Goldberg SN, International Working Group on Image-Guided Tumor Ablation, Standard of Practice Committee of the Cardiovascular and Interventional Radiological Society of Europe. Image-guided tumor ablation: standardization of terminology and reporting criteria–a 10-year update. J Vasc Interv Radiol. 2014;25(11):1691–705. doi:10.1016/j.jvir.2014.08.027.
22. Calmels L, Al-Sakere B, Ruaud JP, Leroy-Willig A, Mir LM. In vivo MRI follow-up of murine tumors treated by electrochemotherapy and other electroporation-based treatments. Technol Cancer Res Treat. 2012;11(6):561–70 **Epub 2012 Jun 15**.
23. Ierardi AM, Lucchina N, Duka E, Bacuzzi A, Dionigi G, Carrafiello G. "Vascular lock" causing splenic perfusion defects during irreversible electroporation of a locally advanced pancreatic tumor. JOP. 2014;15(6):604–8. doi:10.6092/1590-8577/2850.
24. Garrity MM, Burgart LJ, Riehle DL, Hill EU, Sebo TJ, Witzig T. Identifying and quantifying apoptosis: navigating technical pitfalls. Mod Pathol. 2003;16(4):389–94.
25. Niessen C, Igl J, Pregler B, Beyer L, Noeva E, Dollinger M, Schreyer AG, Jung EM, Stroszczynski C, Wiggermann P. Factors associated with short-term local recurrence of liver cancer after percutaneous ablation using irreversible electroporation: a prospective single-center study. J Vasc Interv Radiol. 2015. doi:10.1016/j.jvir.2015.02.001.
26. Wendler JJ, Porsch M, Fischbach F, Pech M, Schostak M, Liehr UB. Letter to the Editor Concerning "Irreversible Electroporation (IRE) Fails to Demonstrate Efficacy in a Prospective Multicenter Phase II Trial on Lung Malignancies: The ALICE Trial" by Ricke et al. 2015. Cardiovasc Intervent Radiol. 2015. doi:10.1007/s00270-014-1049-0.
27. Steinestel J, Steffens S, Steinestel K, Schrader AJ. Positive surgical margins in nephron-sparing surgery: risk factors and therapeutic consequences. World J Surg Oncol. 2014;12:252. doi:10.1186/1477-7819-12-252.
28. Marszalek M, Carini M, Chlosta P, Jeschke K, Kirkali Z, Knüchel R, Madersbacher S, Patard JJ, Van Poppel H. Positive surgical margins after nephron-sparing surgery. Eur Urol. 2012;61(4):757–63. doi:10.1016/j.eururo.2011.11.028.
29. Rendon RA, Kachura JR, Sweet JM, Gertner MR, Sherar MD, Robinette M, Tsihlias J, Trachtenberg J, Sampson H, Jewett MA. The uncertainty of radio frequency treatment of renal cell carcinoma: findings at immediate and delayed nephrectomy. J Urol. 2002;167(4):1587–92.
30. Klingler HC, Marberger M, Mauermann J, Remzi M, Susani M. 'Skipping' is still a problem with radiofrequency ablation of small renal tumours. BJU Int. 2007;99(5):998–1001.
31. Ahmed M, Technology Assessment Committee of the Society of Interventional Radiology. Image-guided tumor ablation: standardization of terminology and reporting criteria–a 10-year update: supplement to the consensus document. J Vasc Interv Radiol. 2014;25(11):1706–8. doi:10.1016/j.jvir.2014.09.005.